Check for updates

The Meteoritical Society

Meteoritics & Planetary Science 55, Nr 10, 2206–2223 (2020)
doi: 10.1111/maps.13570

Characterization of shocked quartz grains from Chicxulub peak ring granites and shock pressure estimates

Jean-Guillaume FEIGNON *[1], Ludovic FERRIÈRE [2], Hugues LEROUX [3], and Christian KOEBERL [1]

[1]Department of Lithospheric Research, University of Vienna, Althanstrasse 14, A-1090, Vienna, Austria
[2]Natural History Museum, Burgring 7, A-1010 Vienna, Austria
[3]Univ-Lille, CNRS, INRAE, Centrale Lille, UMR 8207 – UMET – Unité Matériaux et transformations, 59655 Villeneuve d'Ascq, France
*Corresponding author. E-mail: jean-guillaume.feignon@univie.ac.at

(Received 30 March 2020; revision accepted 14 August 2020)

Abstract–Planar deformation features (PDFs) in quartz are a commonly used and well-documented indicator of shock metamorphism in terrestrial rocks. The measurement of PDF orientations provides constraints on the shock pressure experienced by a rock sample. A total of 963 PDF sets were measured in 352 quartz grains in 11 granite samples from the basement of the Chicxulub impact structure's peak ring (IODP-ICDP Expedition 364 drill core), with the aim to quantify the shock pressure distribution and a possible decay of the recorded shock pressure with depth, in the attempt to better constrain shock wave propagation and attenuation within a peak ring. The investigated quartz grains are highly shocked (99.8% are shocked), with an average of 2.8 PDF sets per grain; this is significantly higher than in all previously investigated drill cores recovered from Chicxulub and also for most K-Pg boundary samples (for which shocked quartz data are available). PDF orientations are roughly homogenous from a sample to another sample and mainly parallel to $\{10\bar{1}3\}$ and $\{10\bar{1}4\}$ orientations (these two orientations representing on average 68.6% of the total), then to $\{10\bar{1}2\}$ orientation, known to form at higher shock pressure. Our shock pressure estimates are within a narrow range, between ~16 and 18 GPa, with a slight shock attenuation with increasing depth in the drill core. The relatively high shock pressure estimates, coupled with the rare occurrence of basal PDFs, i.e., parallel to the (0001) orientation, suggest that the granite basement in the peak ring could be one of the sources of the shocked quartz grains found in the most distal K-Pg boundary sites.

INTRODUCTION

Quartz grains with shock metamorphic features, commonly referred to as "shocked quartz," are a typical diagnostic criterion used for the identification of hypervelocity impact structures on Earth (e.g., Stöffler and Langenhorst 1994; Grieve et al. 1996; French 1998; French and Koeberl 2010; Deutsch et al. 2015; Stöffler et al. 2017; and references therein). In addition to the simple optical properties of quartz and its natural abundance in terrestrial crustal rocks, its shock metamorphic features, forming at a wide pressure range, are well characterized. Upon shock compression, quartz develops irregular fractures (which are not diagnostic shock effects) and several types of planar microstructures, including planar fractures (PFs), feather features (FFs), and planar deformation features (PDFs), all of them being crystallographically controlled (e.g., French and Short 1968; Engelhardt and Bertsch 1969; Stöffler and Langenhorst 1994; Grieve et al. 1996; French 1998; French and Koeberl 2010; Poelchau and Kenkmann 2011; Ferrière and Osinski 2013; and references therein).

Planar fractures start to form at pressures ~>5 GPa; they are parallel open fractures with a spacing of ~15–20 μm or more (see e.g., Stöffler and

[Correction added on 24 October 2020 after first online publication: author name Ludovic FerriÈre is amended with Ludovic Ferrière.]

© 2020 The Authors. *Meteoritics & Planetary Science* published by Wiley Periodicals LLC on behalf of The Meteoritical Society (MET)
This is an open access article under the terms of the Creative Commons Attribution License, which permits use, distribution and reproduction in any medium, provided the original work is properly cited.

Langenhorst 1994; Grieve et al. 1996; French and Koeberl 2010; Ferrière and Osinski 2013; and references therein). Feather features, which are assumed to start to form at pressures ~>7 GPa, are narrowly spaced, short, parallel to subparallel lamellae that branch off of PFs (see Poelchau and Kenkmann 2011). In this study, we focused our attention on PDFs, which start forming ~>8 to 10 GPa and that are composed of narrow, straight, individual planar lamellae (usually less than 200 nm thick) of amorphous material, forming parallel sets spaced 2–10 μm apart (e.g., Engelhardt and Bertsch 1969; Stöffler 1972; Stöffler and Langenhorst 1994). In metamorphosed and altered rocks, PDFs can be recrystallized, but they are still optically visible due to decoration of arrays of small fluid inclusions (Goltrant et al. 1992; Trepmann and Spray 2006).

At pressures higher than 30–35 GPa for non-porous crystalline rocks (such as the samples investigated here), but already at pressures as low as ~5.5 GPa for porous sandstones (Kieffer et al. 1976; Stöffler and Langenhorst [1994] and references therein; Kowitz et al. 2013a, 2013b, 2016), diaplectic quartz glass forms by solid-state transformation, without melting. In porous sandstones and pressures as low as ~7.5 GPa, high-pressure polymorphs of quartz such as coesite and stishovite may form (Mansfeld et al. 2017; Folco et al. [2018], and references therein), whereas for non-porous crystalline rocks, coesite and stishovite form at pressure ranges between 30 and 60 GPa and between 12 and 45 GPa, respectively (e.g., Stöffler and Langenhorst [1994], and references therein). At high temperature (>1500 °C), without necessarily requiring high shock pressures, quartz melts and forms lechatelierite, a monomineralic quartz melt (Stöffler and Langenhorst 1994; French and Koeberl [2010], and references therein).

Planar fractures and PDFs are generally oriented parallel to planes of low Miller–Bravais indices, such as (0001) and $\{10\bar{1}1\}$ for PFs and (0001), $\{10\bar{1}3\}$, and $\{10\bar{1}2\}$ for PDFs (see Ferrière et al. [2009a], and references therein). In crystals showing a (strong) undulose extinction (easily visible under the optical microscope in cross-polarized light), due to a plastic deformation of the crystal lattice (e.g., Trepmann and Spray 2005), the PDFs can look curved. In some rare cases, kinkbands can be seen.

The orientation of PDFs can be characterized and measured using the transmission electron microscope (TEM; e.g., Goltrant et al. 1991), or with a spindle stage (e.g., Bohor et al. 1987) when dealing with single quartz grains. However, to measure and index a large number of PDF sets in a large number of grains in a given sample, only the universal stage (U-stage) technique can be used efficiently; this method is inexpensive, but time consuming if one is to obtain statistically robust, significant, and precise results (see recommendations in Ferrière et al. 2009a; Holm-Alwmark et al. 2018).

The different shock metamorphic features described above and in particular PDFs are important for the investigation of shock pressures experienced by a given rock sample, as the formation of specific PDF orientations depends on the shock pressure, allowing pressure to be derived based on PDF orientation statistics. The shock pressure calibration is based on shock experiments (e.g., Hörz 1968; Müller and Défourneaux 1968). Shock barometry studies have improved the understanding of crater formation processes, in particular shock wave propagation and attenuation with increasing distance from the point of impact, and in some cases to tentatively estimate from which part of the target rock (i.e., sampling horizon) samples were derived before being ejected and incorporated into proximal impactites or even distal ejecta (e.g., Nakano et al. 2008). Moreover, shock barometry results can be integrated to develop and constrain numerical modeling of impact crater, from central uplift (e.g., Ferrière et al. 2008) to peak ring formation (e.g., Rae et al. 2019).

The ~200 km diameter (e.g., Gulick et al. 2013) Chicxulub impact structure, located mostly on the Yucatán peninsula (Mexico), was identified following large-scale negative Bouguer gravity anomaly and magnetic anomalies (Fig. 1). The characterization of shocked quartz grains in samples derived from inside the structure confirmed its impact origin (Penfield and Camargo 1981; Hildebrand et al. 1991). The impact structure is buried under Cenozoic limestones, and the only surface expression of the structure is a ring of cenotes (i.e., water-filled sinkholes). The Chicxulub impact structure, 66.05 Myr old (Sprain et al. 2018), is related to the Cretaceous–Paleogene (K-Pg) boundary, which is evidenced by a distinct ejecta distribution pattern related to distance from the Chicxulub (Alvarez et al. 1980; Smit 1999; Schulte et al. 2010). Impact ejecta material can be found in several K-Pg boundary layers across the world. Shocked quartz grains with PDFs in K-Pg boundary layers were first described by Bohor et al. (1984) and then found in more than 50 K-Pg sites worldwide (e.g., Bohor et al. 1987; Claeys et al. 2002). Chicxulub is the only known impact structure on Earth with a well-preserved, nearly intact, peak ring (80–90 km in diameter), indicated by seismic reflection and refraction surveys (Gulick et al. [2013], and references therein).

Investigating the rocks that make up this peak ring and its nature, chemistry, and origin, as well as its formation mechanism, were some of the primary aims

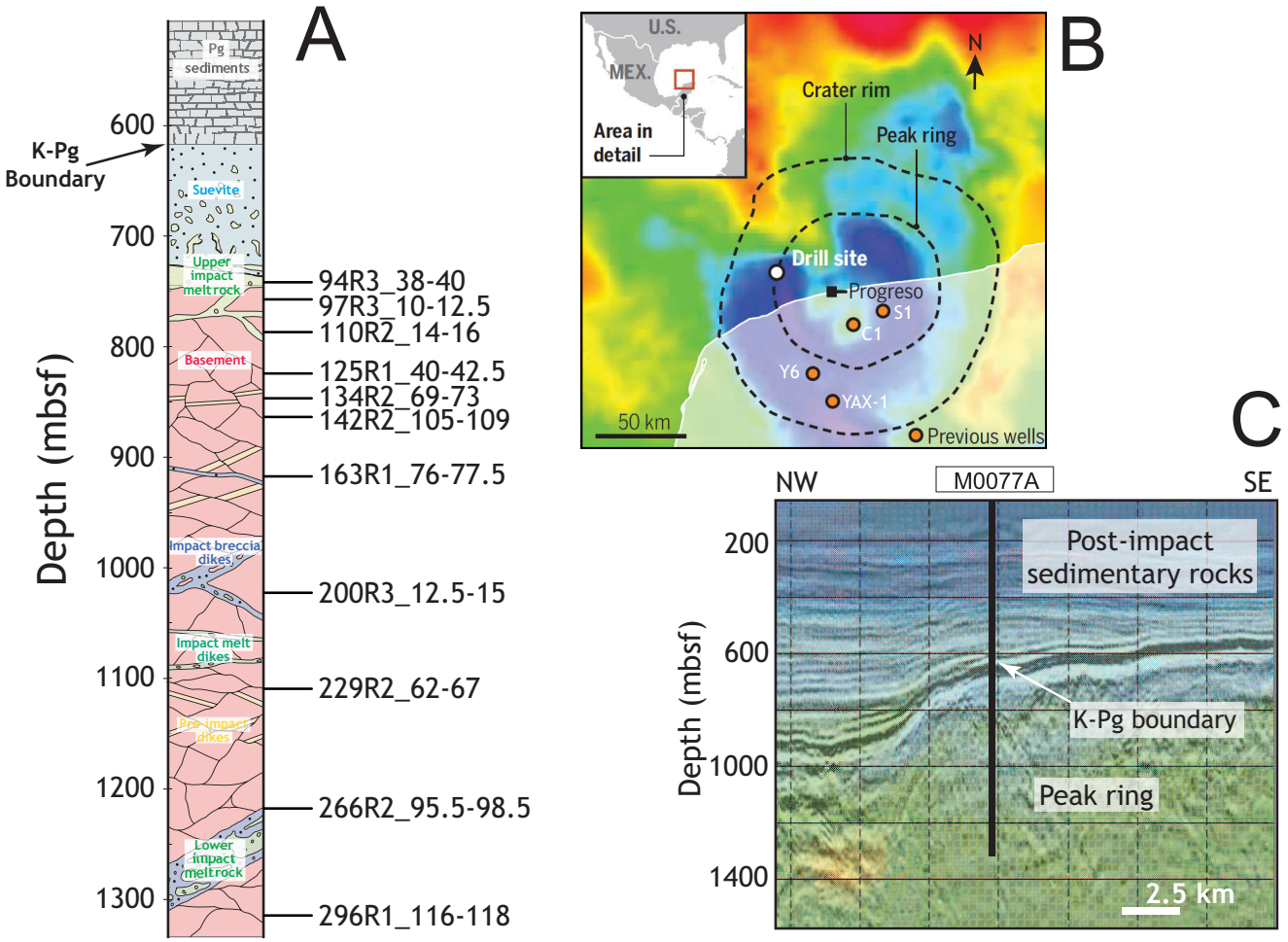

Fig. 1. A) Simplified representation of the stratigraphic log of hole M0077A with the location of the samples that were investigated in this study. Sample references are indicated on the right side of the log (modified from Morgan et al. 2016). B) Drilling site location on the Bouguer gravity anomaly map of the impact structure. Locations of previous drill cores Y6 and YAX-1 are also shown (modified from Hand 2016). C) Radial seismic profile of the peak ring at the drilling site and borehole location (from Morgan et al. 2016). (Color figure can be viewed at wileyonlinelibrary.com.)

of the IODP-ICDP Expedition 364 (Morgan et al. 2017). A continuous core (M0077A) was recovered between 505.7 and 1334.7 mbsf (meters below sea floor). It was divided in three main lithological units (1) a "postimpact" Cenozoic sedimentary rocks section (from 505.7 to 617.3 mbsf), (2) an "upper peak ring" section (from 617.3 to 747.0 mbsf) comprised of ~105 m melt-bearing polymict impact breccia (suevite) overlaying ~25 m of impact melt rocks, and (3) a "lower peak ring" section (from 747.0 to 1334.7 mbsf) consisting of granitoid (coarse-grained granite with aplite and pegmatite facies dikes) intruded by several pre-impact subvolcanic dikes and intercalations of millimeter to decameter suevite and impact melt rocks (Fig. 1). The occurrence of crystalline basement rocks at such depths suggests that they were uplifted at least 2.25 km (Morgan et al. 2016). The peak ring was then intensively altered by a long living, more than 1 Ma, hydrothermal system (Kring et al. 2020).

In this study, we focus on investigations of shocked quartz grains in granite samples recovered from the "lower peak ring" section with the aim to quantify the shock pressure distribution and a possible decay of the recorded shock pressure with depth. The investigated samples represent a large and unique unit of mid-crustal basement rocks (derived from 8–10 km depth; Morgan et al. 2016) that were shocked and then moved outward and upward, then inward before collapsing outward (see e.g., figures in Riller et al. [2018] and Rae et al. [2019]), thus offering the unique opportunity to study and to constrain shock pressures recorded in rocks forming a peak ring as well as to better constrain shock wave propagation and attenuation in a peak ring. In addition, because the

investigated rock unit is possibly one of the sources of shocked quartz grains found in ejecta from numerous K-Pg boundary sites, our results are also here compared with previous PDF measurements published on proximal and distal sites (Nakano et al. [2008], and references therein).

MATERIALS AND METHODS

Forty-one polished thin sections were prepared from a selected number of granite samples taken at regular intervals between 747.0 and 1334.7 mbsf, in the "lower peak ring" section. They were investigated for their shock metamorphic features in quartz and in other minerals using an optical microscope equipped with a U-stage at the University of Vienna and a JEOL JSM-6610 variable pressure (VP) scanning electron microscope (SEM) at the Natural History Museum (Vienna, Austria). An FEI Tecnai G2 20 transmission electron microscope (TEM) on focused ion beam (FIB) foils was also used at the University of Lille (Villeneuve d'Ascq, France) to better characterize the nature of the PDFs. Ten thin sections were selected for additional investigation using the U-stage (Fig. 1; Table 1). In addition, one granite clast in an impact melt rock sample (94R3_38-40) located in the lower part of the "upper peak ring" section, at 743.6 mbsf, was also investigated for comparison, resulting in a total of 11 thin sections investigated. They were selected due to their relative abundance in quartz grains (at least 20 grains per thin section). Additionally, due to the limitations of the U-stage method, quartz grains should be preferentially located in the central part of the thin section to be investigated (i.e., in the case of rectangular thin sections like those that we have investigated here, only about 3/5 of the section can be investigated with the U-stage). In order to obtain reliable statistics on PDF orientations, at least 75 PDF sets were measured for each sample (Ferrière et al. 2009a).

Measurements of the crystallographic orientation of PDFs were obtained using a U-stage (Emmons 1943) mounted on an optical microscope and following the method described in Stöffler and Langenhorst (1994) and Ferrière et al. (2009a). This technique consists of four main steps, including (1) measuring the studied quartz grain *c*-axis; (2) determining the poles perpendicular to planes of all PDFs visible in the quartz grain investigated; (3) plotting on a stereographic Wulff net the *c*-axis and poles to all PDF sets; and (4) indexing, where possible, the PDFs measured using the new stereographic projection template (NSPT), allowing the indexing of 15 typical PDF crystallographic orientations in quartz, within a 5° envelop of measurement error (Ferrière et al. [2009a] and references therein). In this study, *c*-axis and PDF sets were measured twice, that is, the *c*-axis and PDFs are measured, then the inner stage is rotated 180° and the measurements are repeated. This is done in order to avoid measurement errors. For some orientations (*c*-axis and/or PDF sets), a difference of 2–3° was common from the first measurement to the second, inducing in a few cases a slightly higher error than the previously stated 5°. When a set of PDF orientations does not plot inside the envelope of typical PDF orientations from the NSPT, the set is considered as unindexed.

The measurements were indexed using both the manual and the automated methods, using the web-based indexing program (WIP; Losiak et al. 2016). The manual indexing was done at first then using WIP in order to verify the results obtained with the manual indexing method. The manual indexing allows to correct the artificially higher proportion of $\{10\bar{1}4\}$ orientations as found using WIP due to the program failing at considering $\{10\bar{1}4\}$ as a minor orientation, subordinate to the $\{10\bar{1}3\}$ orientation. In case of a measurement in the overlapping area between $\{10\bar{1}4\}$ and $\{10\bar{1}3\}$, the orientation was recorded as $\{10\bar{1}3\}$ (Ferrière et al. 2009a; Holm-Alwmark et al. 2018). In the case of grains displaying a strong undulose extinction, the *c*-axis has to be measured in several areas of the grain, and only the manual indexing method allows us to index the PDFs relative to each other, whereas each measurement has to be considered as a separate grain in WIP.

All the calculated frequencies presented in this study are absolute frequencies, as described by Engelhardt and Bertsch (1969). They are calculated as the number of symmetrically equivalent planes measured in *n* quartz grains, divided by the total number of measured PDF sets in *n* quartz grains.

For assigning average shock pressures to each given sample, the method described in Holm-Alwmark et al. (2018) was used. This method is adapted to estimate shock pressures in non-porous crystalline rocks. To summarize, the average shock pressure for a given sample is derived from a classification of each quartz grain in the sample depending of the measured orientations of PDFs. A shock pressure is assigned to each quartz grain, then a mean value is calculated, giving an average shock pressure for the sample. Holm-Alwmark et al. (2018) defined six different classification types: quartz grains with no PDFs and from A to D types. Quartz grains with no PDFs were assigned a shock pressure of 5 GPa, which is the mean pressure between the onset of shatter cones (2 GPa; e.g., French 1998) and the formation of type A grains. Type A grains (7.5 GPa) contain exclusively basal PDFs (parallel to [0001]). Type B grains (15 GPa) contain PDFs that are parallel to one or more $\{10\bar{1}3\}$- or

Table 1. Petrographic description of the investigated granite samples, based on optical microscopy observations.

Sample	Depth (mbsf)	Lithologies	Main mineral phases	Accessory minerals	Shock/deformation features	Alteration features
94R3_38-40	743.6	Partly digested coarse-grained granite clast (2–3 cm, grain size: ~0.1 to 1.1 cm) included in dark gray, clast-poor (clast size <1 mm) impact melt rock (+some brown greenish veins) with flowing texture Clasts are undigested rock clasts or individual minerals, both with reaction rims Matrix glassy and very finely crystallized (microliths)	Granite: K-Feldspar Quartz Plagioclase Micas (completely decomposed) Impact melt: Clasts: quartz, K-feldspar and plagioclase. Matrix: Microliths of plagioclase and pyroxene	Apatite Titanite Zircon Magnetite (?)	Fractures Microbrecciated areas at the granite rim Quartz shocked with multiple decorated PDF sets, PFs and FFs, toasted and undulose extinction Titanite heavily fractured Ballen quartz (type V; in impact melt rock)	Postimpact calcite filling vesicles (in impact melt rock) and fractures (in granite)
97R3_10-12.5	752.5	Coarse-grained granite (Grain size: ~0.2 to 1.5 cm)	K-feldspar Quartz Plagioclase Biotite (rare and mostly chloritized)	Chlorite Muscovite Apatite Titanite Zircon Epidote Magnetite	Fractures Cataclasite (submillimetric) vein cutting the thin section, microbrecciated quartz, and feldspars (grains subrounded) Some minerals are sheared Quartz shocked with multiple decorated PDF sets, PFs and FFs, undulose extinction, some kinkbanding PFs in feldspars Kinkbanding in biotite Apatite and titanite with planar microstructures	Strong sericitization in feldspars cores, less at the rim Postimpact calcite filling fractures
110R2_14-16	788.1	Coarse-grained granite (Grain size: ~0.1–0.5 cm)	K-feldspar Quartz Plagioclase Chloritized biotite	Chlorite Muscovite Titanite Magnetite Apatite Zircon	Fracturing Small cataclasite vein with microbrecciated shocked quartz and feldspar Shocked quartz with PFs, FFs and decorated PDFs (up to 3 visible, undulose extinction Titanite strongly fractured Kinkbanding common in muscovite and chlorite	Few calcite filling fractures Variable sericitization of feldspar

Table 1. *Continued.* Petrographic description of the investigated granite samples, based on optical microscopy observations.

Sample	Depth (mbsf)	Lithologies	Main mineral phases	Accessory minerals	Shock/deformation features	Alteration features
125R1_40-42.5	826.7	Coarse-grained granite (Grain size: ~0.1–1.2 cm)	K-feldspar Quartz Plagioclase Biotite (chloritized)	Chlorite Muscovite Apatite Titanite Magnetite Zircon	Fracturing Quartz shocked with PFs, FFs, and multiple decorated PDF sets Shearing, PFs, and planar microstructures in feldspar Planar microstructures in apatite Kinkbanding common in biotite-chlorite	Post-impact calcite filling some fractures
134R2_69-73	845.9	Coarse-grained granite (Grain size: 0.5–1.5 cm)	K-feldspar Quartz Plagioclase Biotite (chloritized)	Muscovite Apatite Titanite Epidote Zircon Magnetite	Strong fracturing Shocked quartz with PFs, FFs, and decorated PDFs PFs in feldspar Shearing and strong fracturing in epidote Shearing in apatite Kinkbanding in chlorite/micas	Sericitization of feldspar Postimpact calcite filling fractures
142R2_105-109	861.9	Coarse-grained granite (Grain size: ~0.5–1.0 cm)	K-feldspar Quartz Plagioclase Biotite (rare and chloritized)	Chlorite Titanite Apatite Magnetite	Fracturing Shocked quartz with PFs, FFs, and decorated PDFs (2–3 sets commonly visible), undulose extinction PFs (up to 2 sets) and planar microstructures in feldspar Clear planar microstructures in titanite	Variable sericitization of feldspar Some postimpact filling in calcite
163R1_76-77.5	915.5	Coarse-grained granite (Grain size ~0.5–1.5 cm)	K-feldspar Quartz Plagioclase Biotite (strong chloritization)	Chlorite Titanite Magnetite Zircon Monazite [?]	Shocked quartz with PFs, FFs, and slightly decorated PDFs (up to 3 sets observed), undulose extinction Fracturing and planar microstructures in feldspar, titanite	Sericitization common in feldspar Some fractures filled with opaque minerals
200R3-12.5-15	1021.0	Coarse-grained granite (Grain size: ~0.2–0.8 cm)	K-feldspar Quartz Plagioclase Biotite (rare and often chloritized)	Chlorite Muscovite Apatite Titanite Zircon Epidote Magnetite	Fracturing Thin cataclastic areas with microbrecciated quartz and feldspar (subrounded) Quartz with PFs, FFs, and decorated PDFs, low undulose extinction Kinkbanding (common) in micas/chlorite Planar microstructures in apatite (2 sets) and titanite	Strong sericitization in some feldspars Postimpact calcite filling fractures

Table 1. *Continued.* Petrographic description of the investigated granite samples, based on optical microscopy observations.

Sample	Depth (mbsf)	Lithologies	Main mineral phases	Accessory minerals	Shock/deformation features	Alteration features
229R2_62-67	1107.2	Coarse-grained granite (Grain size: <0.1–1.3 cm)	K-feldspar Quartz Plagioclase	Muscovite Chlorite Apatite Titanite Epidote (Fe) Magnetite Zircon Monazite (?)	Open fracture Quartz with PFs, FFs, and decorated PDFs, K-feldspar with PFs, and planar microstructures Planar microstructures in apatite and titanite Kinkbanding in micas/chlorite (common) Shearing in feldspar, apatite	Sericitization in feldspar Some postimpact calcite
266R2_95.5-98.5	1220.5	Coarse-grained granite (Grain size: < 0.8 cm)	K-feldspar Quartz Plagioclase Biotite	Muscovite Chlorite Opaque minerals (Magnetite [?]) Apatite Epidote Titanite	Strong fracturing, few shearing Cataclasite area with quartz, feldspar, and opaque minerals no mineral deformation Shocked quartz with PFs, FFs, and decorated PDFs (1–2 sets visible) Planar microstructures in feldspar Kinkbanding and fracturing (common) in biotite	Some sericitization in plagioclase Fracture filling with opaque minerals Low chloritization of biotite
296R1_116-118	1311.1	Coarse-grained granite (Grain size: ~0.5–1.5 cm)	K-feldspar Quartz Plagioclase	Few/tiny accessory phases Chlorite (former biotite) Muscovite Apatite Magnetite Zircon	Thin cataclasite veins with shocked minerals (quartz and felsdpar) Strong fracturing Shearing in minerals Shocked quartz with PFs, FFs, and decorated PDF sets (at least 2 visible), common undulose extinction Kinkbanding in plagioclase and rare in quartz	Postimpact calcite filling fractures and partially filling PFs in quartz Some sericite in plagioclase

{10$\bar{1}$4}-equivalent plane(s). Type B2 grains (16.5 GPa) contain three or more PDFs with {10$\bar{1}$3}- or {10$\bar{1}$4}-equivalent planes. Type C grains (17 GPa) contain PDFs with high index orientation(s), such as {11$\bar{2}$2} and/or {22$\bar{4}$1}, and type D grains (20 GPa) contain PDFs parallel to one or more {10$\bar{1}$2}-equivalent orientation(s). An additional type, type E, was added by Fel'dman (1994) corresponding to quartz grains transformed to diaplectic glass. However, no type E grains were identified in any of the investigated samples.

RESULTS AND DISCUSSION

Sample Descriptions

The investigated samples mainly consist of pervasively deformed, locally micro-brecciated (presence of cataclastic veins) and sheared, coarse-grained leucogranite (Fig. 2). The grain size ranges from ~0.2 to 4 cm, but also submillimeter-sized grains occur in cataclasite veins crosscutting some of the granite samples. Some of the cataclasites exhibit a greenish color, due to a hydrothermal overprint (Kring et al. 2020). The mineral assemblage consists mainly of K-feldspar (orthoclase, ~25–40%); plagioclase (~25–35%), which is often highly sericitized; quartz (~25–35%); and, to a lesser extent, biotite (~1–5%), often chloritized. The main accessory minerals are muscovite, (fluor)apatite, titanite, epidote (piemontite), zircon, (titano)magnetite, and allanite. Other accessory minerals, including monazite, ilmenite, rutile, chalcopyrite, cobaltoan pyrite, stolzite/raspite, galena, uranothorite, and uranothorianite, were also detected during our SEM survey. Shock features were observed in alkali-feldspar and plagioclase (i.e., PFs filled with opaque minerals and also some possible PDFs; see Pittarello et al. 2020), titanite, and apatite (with different types of planar microstructures; Timms et al. 2019; Cox et al. 2020). Kinkbanding is common in biotite, muscovite, and chlorite, and is also observed, to a lesser extent, in plagioclase and quartz. Postimpact calcite veinlets commonly cut the granite (see details in Table 1).

The investigated granite clast (3.5 cm in size) in sample 94R3_38-40 occurs in a dark-greenish, clast-poor, impact melt rock sample. Other clasts in this impact melt rock sample (<1 mm size) include granite and mineral clasts, such as K-feldspar, plagioclase, shocked quartz (with PDFs, some toasted), and ballen silica of type V (i.e., characterized by a chert-like texture that formed following a complete recrystallization of the ballen; see Ferrière et al. 2009b), and, to a lesser extent, calcite (see Table 1).

In the selected thin sections, a total of 352 quartz grains were investigated. Nearly all (99.8%) of the observed grains are shocked (only one apparently unshocked quartz grain was seen during our survey), including PFs with (or without) FFs and PDFs (up to 7 sets of PDFs as seen under the U-stage). In addition, almost all quartz grains show undulose extinction which can be occasionally extreme, and in a few cases kinkbands (Fig. 3). As seen under the optical microscope and further documented under the SEM, the PFs enhance fluid circulation inside the grains as shown by the corroded margins of the PFs and the presence of postimpact, secondary calcite filling the PFs. Similar observations were made by Kring et al. (2020) on granite samples from the peak ring. The PDFs are decorated with trails of vugs or tiny fluid inclusions. The TEM observations allow us to resolve the PDFs at high magnification, showing that they are composed of aligned fluid inclusions or vugs and dislocations (Fig. 3), microstructures typical of annealed PDFs. Free dislocations and subgrain boundaries were also observed. Dislocations preferentially occur along the fluid inclusions trails. No glass-bearing lamellae were detected in the investigated samples. The observation that PDFs are annealed and decorated indicates that the originally amorphous PDFs were recrystallized during a postshock thermal episode. Kinkbanding of some shocked quartz grains shows that, after the propagation of the shock wave and formation of the PDFs, the granitoids from the "lower peak ring" section were subject to intense stress and were sheared, as also indicated by mineral-specific fracturing and localized cataclasites (Rae et al. 2019).

Crystallographic Orientations of the PDFs

The U-stage was used to characterize the crystallographic orientation of both PFs and PDFs in quartz grains. In total, 963 sets of PDF (and 97 sets of PF) were measured in 352 quartz grains, resulting in an average of ~2.8 PDF sets per grain (see Table 2).

PFs are mainly oriented parallel to {10$\bar{1}$1} (~60%), (0001) (~20%), and, to a lesser extent, to {10$\bar{1}$3} (~8%) orientations.

Figure 4 and Table 3 show the PDFs orientation frequencies and the proportion of unindexed sets. Our measurements for all the granite samples, including also the granite clast in impact melt rock, show that PDFs with {10$\bar{1}$3} and {10$\bar{1}$4} orientations are most abundant, together representing 68.6% of the total measured orientations. Then, by decreasing abundances, PDFs parallel to {10$\bar{1}$2} (7.4%), {10$\bar{1}$1} (3.7%), {11$\bar{2}$2} (3.1%), and {22$\bar{4}$1} (3.0%) occur, with variations from sample to sample (see Fig. 4 and Table 3). Other orientations have frequencies below 2% with only a few basal PDFs (i.e., parallel to [0001]; 1.7%). No PDFs with {51$\bar{6}$0} orientation were observed in our survey.

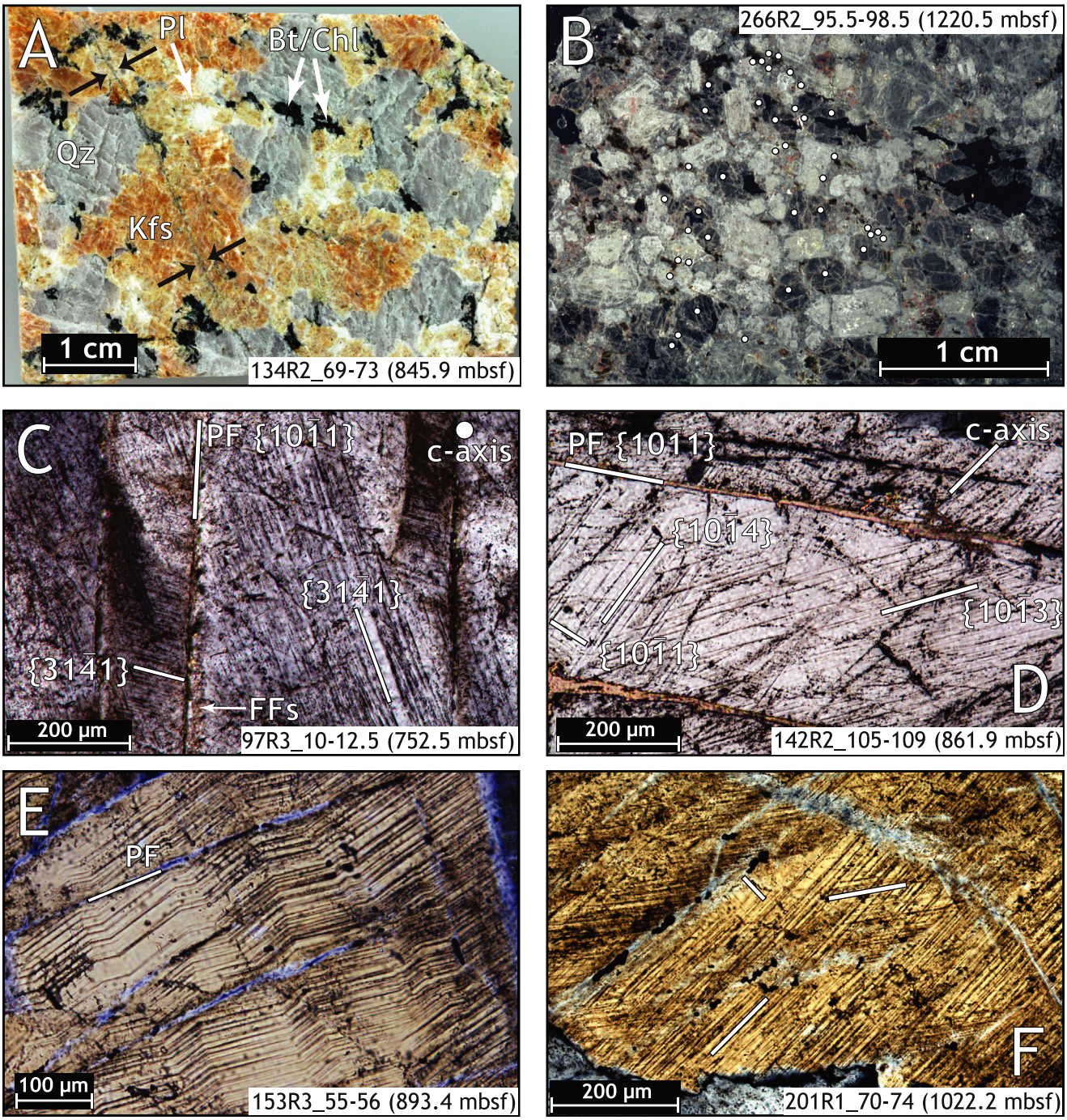

Fig. 2. Macrophotograph (A) and thin section scan (B) of typical coarse-grained granite samples from the "lower peak ring" section that were investigated in this study. See Table 1 for the petrographic descriptions. A) All minerals are highly fractured. A thin greenish (hydrothermally altered) cataclasite vein cross-cut the sample on the left side (black arrows). Bt: biotite, Chl: chlorite, Kfs: K-feldspar, Pl: plagioclase, and Qz: quartz. B) Thin section scan of one of the granite samples investigated under the U-stage. The white dots indicate the positions of the investigated quartz grains. Thin section photomicrographs of shocked quartz grains (all in cross polarized light). C) Shocked quartz with one set of PF with branched FFs and two sets of decorated PDFs; as indicated, the *c*-axis of the grain is perpendicular to the field of view. The deformation of the crystal is evidenced with the undulose extinction. D) Quartz grain with one set of PF filled with postimpact calcite and three sets of decorated PDFs. E) Shocked quartz with kinkbanding. As the kinkbanding affected both PF and PDF, it must have occurred after the onset of PF and PDF formation (this specific sample was not measured with U-stage). F) Shocked quartz grain with two prominent decorated PDF sets and a third set of PDFs that are barely visible in this photograph, but are indicated with a white mark (sample not measured with the U-stage). (Color figure can be viewed at wileyonlinelibrary.com.)

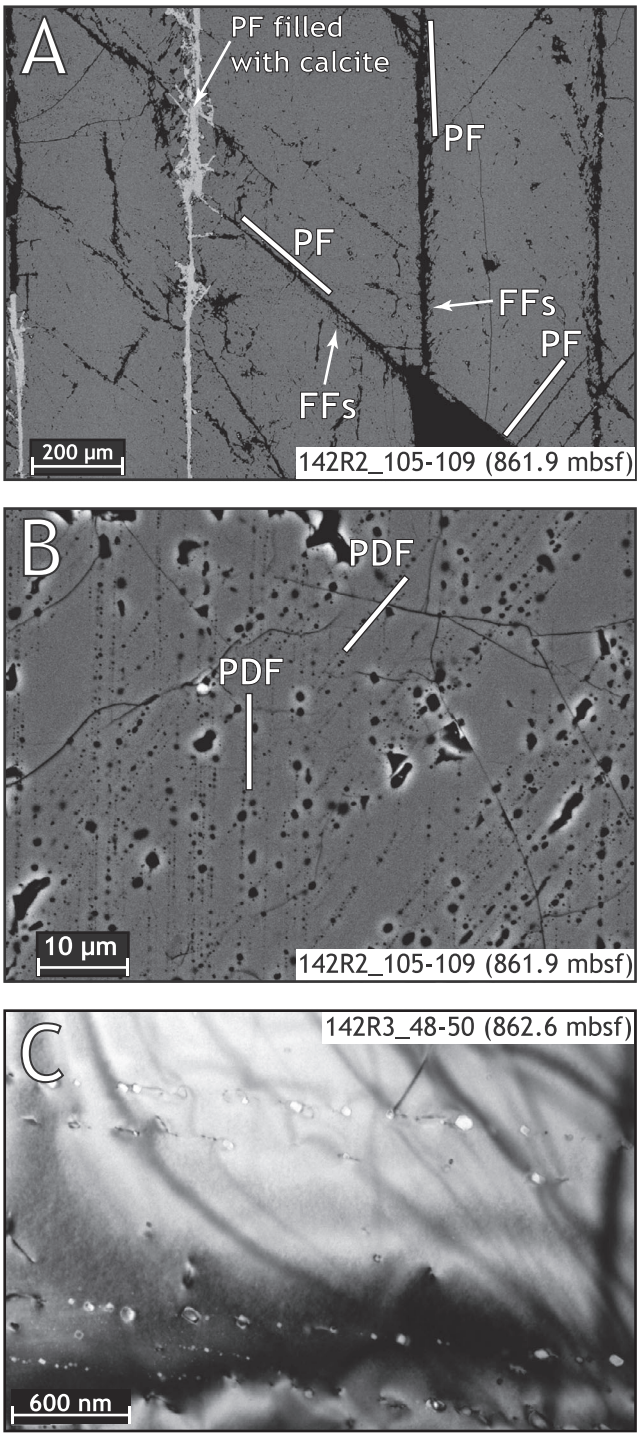

Fig. 3. A and B) SEM backscattered electron (BSE) images of shocked quartz grains from sample 142R2_105-109. A) Shocked quartz grain with three sets of PFs, including one set filled with postimpact calcite. The FFs are also evidenced, branching off the PFs. Note in both PFs and FFs cases the dissolution of quartz at the margins. B) Two sets of highly decorated PDFs. C) Bright field transmission electron microscope (TEM) micrograph of a quartz grain with one set of decorated PDFs. Aligned fluid inclusions or vugs are visible as well as dislocations, preferentially occurring along the vugs/fluid inclusions.

The frequency of unindexed sets is below 15%, on average of 6.1%, which is reasonable considering that quartz grains often exhibit strong undulose extinction. Only one sample (296R1_116-118) has nearly 15% of unindexed sets as it was the first sample investigated using the U-stage by J.-G. F. In order to confirm the reliability of the data, the sample 200R3_12.5-15 was measured twice, by two different users with varying experience. The results gave a similar pattern, except for the $\{22\bar{4}1\}$ orientation, which was slightly more abundant in the second measurement, but this minor difference does not affect the shock pressure estimate.

The PDF orientation frequencies for all the samples are broadly similar, with some outliers. The granite clast sample (sample 94R3_38-40) shows a pattern very similar to the one of the upper samples, except for the $\{11\bar{2}1\}$ orientation, which is significantly more abundant, representing 6.4% of the total, to be compared to less than 2% for the other samples of the upper part of the investigated granite unit. Interestingly, an increase in the $\{10\bar{1}2\}$ orientation frequency is seen with decreasing depth. A similar trend is also observed, to a lesser extent, for the $\{11\bar{2}2\}$ and $\{22\bar{4}1\}$ orientations.

The majority of the investigated quartz grains have three sets of PDFs, representing on average 34.7% of the total (see Fig. 5), whereas the quartz grains with two sets of PDFs represent on average 29.0% of the total. The average number of PDF sets per grain seems to slightly decrease with increasing depth (see Table 3 and Fig. 6). The three deepest samples investigated have mainly shocked quartz grains with two sets of PDFs, representing from 36.8% to 48.6% of the total, whereas the shallowest samples in the unit have a majority of quartz grains with three sets of PDFs, representing from 30.4% to 48.1% of the total. The sample 97R3_10-12.5 shows a higher proportion of quartz grains with four sets of PDF (representing 26.5% of the total) than all the other investigated samples whereas the granite clast sample has a significantly higher abundance of quartz grains with five sets of PDFs (representing 30.4% of the total). All these observations are indicative of a slight decrease of the shock intensity with increasing depth in the core.

Shock Pressure Estimates

Based on our U-stage results, and following the shock pressure estimation model of Holm-Alwmark et al. (2018), the granites from the "lower peak ring" section record shock pressures between ~16 and 18 GPa (see Table 3 and Fig. 6). Our shock pressure estimates are consistent with observations published on zircon grains from the same granite unit, indicating that the shock pressure was <20 GPa (Timms et al. 2019). In

Table 2. Summary of PDF set abundances in quartz grains and results of our universal-stage investigations of 11 thin sections of granites from the Chicxulub impact structure peak ring.

Sample	Depth (mbsf)	Number of grains	% grains with PDFs	Number of sets	Average number of sets/grain
94R3_38-40[a]	743.6	23	100	78	3.4
97R3_10-12.5	752.5	34	100	97	2.9
110R2_14-16	788.1	34	100	102	3.0
125R1_40-42.5	826.7	23	100	72	3.1
134R2_69-73	845.9	29	100	91	3.1
142R2_105-109	861.9	27	100	79	2.9
163R1_76-77.5	915.5	27	100	78	2.9
200R3-12.5-15	1021.0	38	100	90	2.4
229R2_62-67	1107.2	39	97.4	111	2.8
266R2_95.5-98.5	1220.5	43	100	84	2.0
296R1_116-118	1311.1	35	100	81	2.3
Total		352	99.8	963	2.8

[a]Granite clast in impact melt rock.

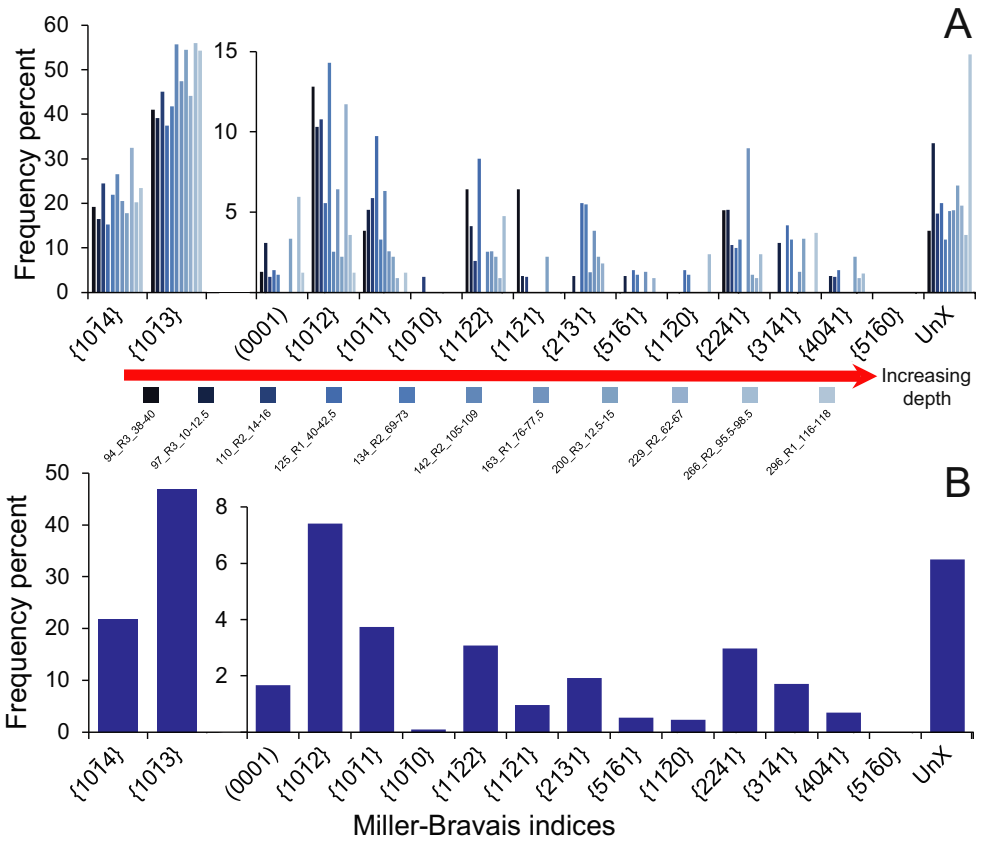

Fig. 4. A and B) Histograms showing the absolute frequencies of PDF orientations (Miller–Bravais indices). With the exception of the (0001) orientation, all the orientations are ranked with increasing angle between the *c*-axis and the pole to PDFs. UnX = unindexed. A) Detailed histogram for each investigated sample, with increasing depth from the darkest to the lightest bar (i.e., from left to right). B) Histogram showing a compilation of all our measurements. (Color figure can be viewed at wileyonlinelibrary.com.)

addition, a shock pressure range of ~16–18 GPa is also in good agreement with the presence of TiO_2-II as described by Schmieder et al. (2019). Although the range of pressure estimates is very narrow, taking into account the errors associated with the measurements, a slight shock attenuation with increasing depth is

Table 3. Crystallographic orientation abundances of PDFs (%) derived from universal-stage measurements of shocked quartz grains in granites from the Chicxulub impact structure peak ring and shock pressure estimates.

Sample	Depth (mbsf)	*c* (0001)	{10$\bar{1}$4}	ω, ω′ {10$\bar{1}$3}	π, π′ {10$\bar{1}$2}	r, z {10$\bar{1}$1}	m {10$\bar{1}$0}	ξ {11$\bar{2}$2}	s {11$\bar{2}$1}	ρ {21$\bar{3}$1}	x {51$\bar{6}$1}	a {11$\bar{2}$0}	{22$\bar{4}$1}	{31$\bar{4}$1}	t {40$\bar{4}$1}	k {51$\bar{6}$0}	Unindexed	Average shock pressure (GPa)[b]
94R3_38-40[a]	743.6	1.3	19.2	41.0	12.8	3.9	n.d.	6.4	6.4	n.d.	n.d.	n.d.	5.1	n.d.	n.d.	n.d.	3.9	17.7
97R3_10-12.5	752.5	3.1	16.5	39.2	10.3	5.2	n.d.	4.1	1.0	1.0	1.0	n.d.	5.2	3.1	1.0	n.d.	9.3	17.2
110R2_14-16	788.1	1.0	24.5	45.1	10.8	5.9	1.0	1.9	1.0	n.d.	n.d.	n.d.	2.9	n.d.	1.0	n.d.	4.9	17.4
125R1_40-42.5	826.7	1.4	15.3	37.5	5.6	9.7	n.d.	8.3	n.d.	5.6	1.4	1.4	2.8	4.2	1.4	n.d.	5.6	17.0
134R2_69-73	845.9	1.1	22.0	41.8	14.3	3.3	n.d.	n.d.	n.d.	5.5	1.1	1.1	3.3	3.3	n.d.	n.d.	3.3	17.6
142R2_105-109	861.9	n.d.	26.6	55.7	2.5	6.3	n.d.	2.5	n.d.	1.3	n.d.	n.d.	n.d.	n.d.	n.d.	n.d.	5.1	16.6
163R1_76-77.5	915.5	n.d.	20.5	47.4	6.4	2.6	n.d.	2.6	n.d.	3.8	1.3	n.d.	9.0	1.3	n.d.	n.d.	5.1	17.0
200R3_12.5-15	1021.0	3.3	17.8	54.4	2.2	2.2	n.d.	2.2	2.2	2.2	n.d.	n.d.	1.1	3.3	2.2	n.d.	6.7	16.2
229R2_62-67	1107.2	n.d.	32.4	44.1	11.7	0.9	n.d.	0.9	n.d.	1.8	0.9	n.d.	0.9	n.d.	0.9	n.d.	5.4	17.0
266R2_95.5-98.5	1220.5	6.0	20.2	56.0	3.6	n.d.	n.d.	4.8	n.d.	n.d.	n.d.	2.4	2.4	n.d.	1.2	n.d.	3.6	15.8
296R1_116-118	1311.1	1.2	23.5	54.3	1.2	1.2	n.d.	n.d.	n.d.	n.d.	n.d.	n.d.	n.d.	3.7	n.d.	n.d.	14.8	15.8
Average all samples		1.7	21.7	47.0	7.4	3.7	0.1	3.1	1.0	1.9	0.5	0.4	3.0	1.7	0.7	n.d.	6.1	16.8

[a]Granite clast in impact melt rock.
[b]Using Holm-Alwmark et al. (2018) calibration.

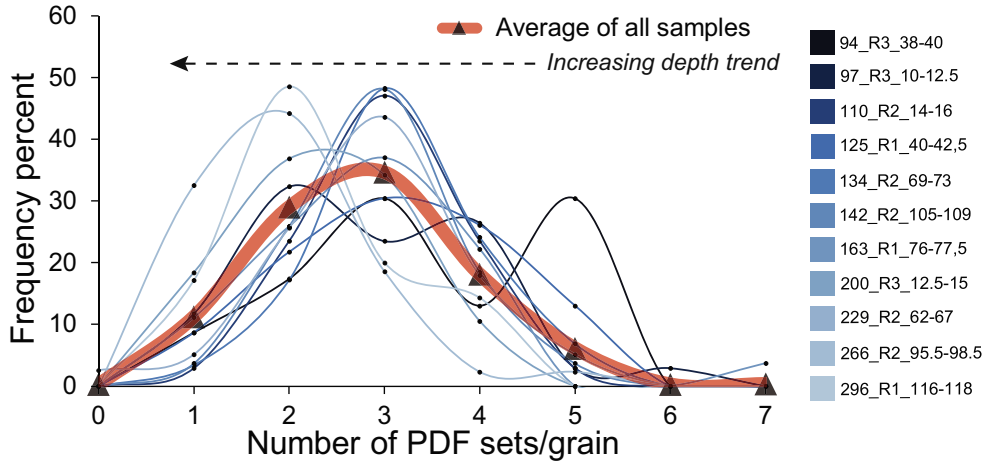

Fig. 5. Frequency of the number of PDF sets per grain for each investigated sample (same color code as for Figure 4). The average abundance for all sample is shown as bold curve and black triangles. There is a clear decrease in the abundance of shocked quartz grains with three sets of PDFs with increasing depth whereas the proportion of shocked quartz grains with two sets of PDFs increases inversely. The granite clast in impact melt rock sample 94R3_38-40 is clearly distinguishable here, with a significantly higher abundance of shocked quartz grains with five sets of PDFs (i.e., representing 30.4%). (Color figure can be viewed at wileyonlinelibrary.com.)

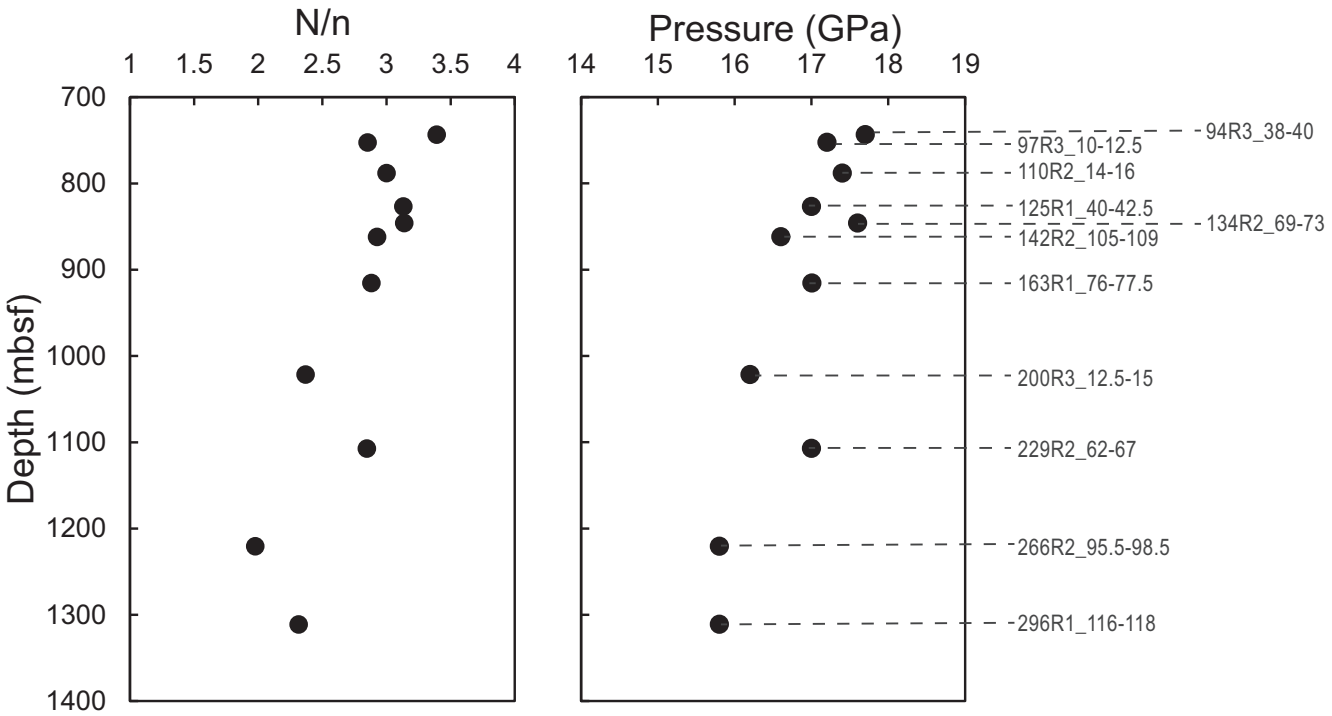

Fig. 6. Average number of PDF sets per grain (i.e., N/n, with N the number of PDF sets/grain and n the number of measured quartz grains; left) and estimated shock pressure (right) for each sample versus depth. In both cases, a slightly, but significant, decreasing of the values with increasing depth is visible, indicating a slight shock attenuation with increasing depth within the "lower peak ring" granite basement. Sample 229R2_62-67 is somewhat out of the general trend (i.e., it shows a slightly higher shock pressure than the neighbor samples), likely due to the fact that the thin section was prepared from a granite that is in direct contact with an aplite (i.e., the thin section was prepared at less than 1 cm from the contact), and such a textural change can induce a slight pressure excursion.

noticeable. The observed slight shock attenuation is highlighted by the abundance of PDFs parallel to the $\{10\bar{1}2\}$ orientation, that is, known to form at pressures of at least 20 GPa (Hörz 1968), significantly more abundant in the upper section of the granite basement (representing between 6% and 14% of the total) than in

the lower section (representing less than 3% of the total). The slight shock attenuation with increasing depth is also supported by the decreasing abundance of quartz grains with three sets of PDFs with increasing depth (see Fig. 6). This further supports the suggestion that the upper section of the granite basement experienced slightly higher shock pressures than the lower section.

The granite clast in impact melt rock located just on top of the granite unit rock investigated here recorded the highest shock pressure (17.7 GPa) of all the investigated samples. This is not surprising because this clast is derived from a section shocked at higher pressures that was either assimilated in the impact melt or that was ejected.

In general, our shock pressure estimates are slightly lower than the shock pressures derived from the dynamic collapse model for peak ring formation as modeled for the Chicxulub impact structure by Rae et al. (2019). In this model, the peak shock pressure calculated during the shock and decompression stage for the peak ring material is 22.2 GPa. This suggests either that the modeled peak shock pressures for the peak ring material are slightly overestimated or that the investigated "lower peak ring" granite was derived from a somewhat different area from the peak ring that experienced slightly lower shock pressure than the area selected in the model by Rae et al. (2019). In any case, our results can be used in order to further constrain the peak ring formation model.

Comparison with Previous Studies

The average abundance of shocked quartz grains in the investigated samples is 99.8% of the total number of quartz grains. This is significantly higher than the abundance of shocked quartz grains reported in previous studies of several K-Pg boundary sites worldwide. In terrestrial (non-marine) K-Pg sites, a very low number, from less than 2% (see Morgan et al. 2006; Nakano et al. 2008) to as much as ~25%, of the quartz grains are shocked (see Bohor et al. 1984, 1987; Izett 1990). Samples from oceanic drill cores recovered in the Atlantic and in the Pacific show on average a much higher abundance of shocked quartz grains, with about 36% and 23%, respectively (Morgan et al. 2006), and up to 63% in some Pacific sites according to Bostwick and Kyte (1996). The large difference in the abundance of shocked quartz grains from a study to another for the same geographical area can be explained by differences in the used protocols (e.g., sample selection, separation technique used, and preparation). Thus, comparison of different studies and derived numbers/proportions can be challenging. For example, the estimated dilution of the proportion of shocked quartz grains by detrital quartz can vary significantly (Morgan et al. 2006). Interestingly, the fraction of shocked quartz grains reported for suevites from drill cores YAX-1 (Nakano et al. 2008) and Y6 (Sharpton et al. 1992), both recovered within the impact structure, is 31% and 33%, respectively. Only at K-Pg sites in the United States and Canada, the abundance of shocked quartz grains is much higher, but still lower compared to the samples investigated in this work, with ~80% of the quartz grains being shocked (Morgan et al. 2006).

The average number of PDF sets per grain recorded in the peak ring granite samples is also higher than in any other previously studied K-Pg boundary sites and drill cores in which an average from 1.4 to 2 PDF sets/grain were observed (Grieve and Alexopoulos 1988; Morgan et al. 2006; Nakano et al. 2008). Only the shocked quartz grains in Y6 drill core, with an average of 2.4 PDF sets/grain (Sharpton et al. 1992), and in some Western U.S. K-Pg sites, with an average of 2.8 PDF sets/grain (Izett 1990), show values approaching or similar to those that we have obtained from the investigated granite unit. Bohor et al. (1984, 1987) reported a higher average number of "planar features," 4.1 and 3.5, respectively, but it is not clear if all these features were indeed PDFs.

The PDF orientations and their abundances in our study show patterns generally similar to those obtained for distal K-Pg sites in Europe, the Pacific Ocean, North America, and in the YAX-1 drill core (Badjukov et al. 1986; Bohor et al. 1987; Grieve and Alexopoulos 1988; Izett 1990; Bostwick and Kyte 1996; Nakano et al. 2008) with the $\{10\bar{1}3\}$ orientation being the most abundant one, followed by the $\{10\bar{1}2\}$ orientation. It should be noted that in most studies published before 2009, the $\{10\bar{1}4\}$ orientation was not considered (i.e., some of these orientations were indexed as $\{10\bar{1}3\}$ orientations, other were unindexed), as it was only introduced later by Ferrière et al. (2009a). Another striking similarity between our results and those obtained for distal ejecta and YAX-1 samples is the absence or very low abundance of basal PDFs, parallel to (0001).

Interestingly, in two proximal K-Pg boundary sites investigated by Nakano et al. (2008; i.e., Moncada and Peñalver Formations, in Mexico), both located less than 800 km away from the center of the Chicxulub impact structure, the abundance of basal PDFs is up to 7.0% of the total measured orientations, and a similar abundance was found in the suevite unit from the Y6 drill core (Y6-N14) as reported by Sharpton et al. (1992). It was suggested by Nakano et al. (2008) that because PDFs with the (0001) orientation develop at the

lowest shock pressure (i.e., ~7.5 GPa), these shocked quartz grains were derived from lower shock pressure zones than the other grains derived from more central parts of the crater. Moreover, the formation of basal PDFs parallel to the (0001) plane, which represents mechanical Brazil micro-twin lamellae, requires a shear component, whereas other PDF orientations do not (e.g., Goltrant et al. 1991, 1992; Trepmann and Spray 2005). The difference in terms of recorded shock pressures between YAX-1 and Y6 drill cores is likely the result of a different sampling horizon. In addition, an increase of the recorded shock pressure in distal ejecta with increasing distance from the crater was evidenced either by the increasing average number of PDF sets/grain (Morgan et al. 2006) or by the increasing abundance of orientations that are known to form at higher shock pressures (Alvarez et al. 1995; Nakano et al. 2008). Shock pressures recorded for the quartz grains in this study are very similar to those recorded for quartz grains from distal K-Pg sites. Consequently, we can assume that the lower peak ring granite is probably the source material for the shocked quartz grains found in distal K-Pg boundary sites. The occurrence of spinel group minerals (picotite) at some of the distal K-Pg sites also suggests that some grains originate from the crystalline portion of the Chicxulub peak ring, that is, were derived from pre-impact dikes of dolerite as suggested by Schmieder et al. (2017). However, a comparison of our results with existing published data is somewhat challenging. Shocked quartz grains investigated in K-Pg sites and in previous drill cores occur as single, submillimetric grains in sedimentary (calcareous clastic, clays) deposits or suevite, whereas the shock quartz grains investigated in this study are generally larger, up to 15 mm in size, and from a crystalline (granitic) basement that was not reworked by any sedimentary process that may induce a significant dilution with local detrital unshocked quartz grains (i.e., what would affect the relative abundance of shocked quartz grains in a given unit, but not the PDF orientations nor the average number of PDF sets per grain; Claeys et al. 2002; Morgan et al. 2006). Moreover, comparing PDF orientations is not straightforward due to somewhat different methodologies used and the way the data are presented.

CONCLUSIONS

Our observations and results on shocked quartz grains confirm that the rocks of the granite basement unit in the Chicxulub impact structure peak ring are moderately shocked, as is indicated by the high abundance of shock features, such as PFs, FFs, and PDFs in quartz. The PDF orientation distribution patterns in the peak ring granite are very similar to the distribution for distal K-Pg sites and the YAX-1 drill core, with the $\{10\bar{1}3\}$ orientations being the most abundant orientation and a very low abundance of basal PDFs compared to more proximal samples, that is, less than 800 km away from crater center (Nakano et al. 2008) and in the Y6 drill core (Sharpton et al. 1992), suggesting that the "lower peak ring" granite is possibly the source material of the shocked quartz grains found in distal K-Pg boundary sites.

Almost all quartz grains investigated are shocked at pressures between ~16 and 18 GPa, with a slight shock attenuation with increasing depth, highlighted by the increasing abundance of PDFs parallel to $\{10\bar{1}2\}$ orientation, known to develop at higher shock pressures (Hörz 1968) and the increasing average number of PDF sets per grain with decreasing depth. The abundance of shocked quartz and the average number of PDF sets per grain in this study is somewhat higher than in samples recovered in previous Chicxulub drill cores and from most K-Pg boundaries.

Acknowledgments—This paper is dedicated to the memory of Bruce F. Bohor (1932–2019), who first described the occurrence of shocked quartz grains in the Cretaceous–Paleogene boundary layer. The Chicxulub drilling was funded by the IODP as Expedition 364, with co-funding from ICDP. Expedition 364 was implemented by ECORD, with contributions and logistical support from the Yucatán state government and Universidad Nacional Autónoma de México. Partial funding was provided by the University of Vienna doctoral school IK-1045 (P.I.: C.K.). H.L. thanks the Renatech platform and David Troadec for the FIB preparation. The TEM facility in Lille (France) is supported by the Conseil Régional du Nord-Pas-de-Calais, and the European Regional Development Fund (ERDF). A. Rae and L. Pittarello are acknowledged for interesting discussions based on limited U-stage data they have also obtained for a few samples from the IODP-ICDP Expedition 364. We thank C. Alwmark and M. Schmieder for constructive reviews and J. Plescia for editorial handling.

Editorial Handling—Dr. Jeffrey Plescia

REFERENCES

Alvarez L. W., Alvarez W., Asaro F., and Michel H. V. 1980. Extraterrestrial cause for the Cretaceous-Tertiary extinction. *Science* 208:1095–1108.

Alvarez W., Claeys P., and Kieffer S. W. 1995. Emplacement of K/T boundary shocked quartz from Chicxulub crater. *Science* 269:930–935.

Badjukov D. D., Nazarov M. A., and Suponeva I. V. 1986. Shocked quartz grains from K/T boundary sediments

(abstract). 17th Lunar and Planetary Science Conference. pp. 18–19.

Bohor B. F., Foord E. E., Modreski P. J., and Triplehorn D. M. 1984. Mineralogic evidence for an impact event at the Cretaceous-Tertiary boundary. *Science* 224:867–869.

Bohor B. F., Modreski P. J., and Foord E. E. 1987. Shocked quartz in the Cretaceous-Tertiary boundary clays: Evidence for a global distribution. *Science* 236:705–708.

Bostwick J. A. and Kyte F. T. 1996. The size abundance of shocked quartz in Cretaceous-Tertiary boundary sediments from the Pacific Basin. In *The Cretaceous-Tertiary event and other catastrophes in Earth history*, edited by Ryder G., Fastovsky D., and Gartner S. Geological Society of America Special Paper 307. Boulder, Colorado: Geological Society of America. pp. 403–415.

Claeys P., Kiessling W., and Alvarez W. 2002. Distribution of Chicxulub ejecta at the Cretaceous-Tertiary boundary. In *Catastrophic events and mass extinctions: Impact and beyond*, edited by Koeberl C. and MacLeod G. Geological Society of America Special Paper 356. Boulder, Colorado: Geological Society of America. pp. 55–68.

Cox M. A., Erickson T. M., Schmieder M., Christoffersen R., Ross D. K., Cavosie A. J., Bland P. A., Kring D. A., and IODP–ICDP Expedition 364 Scientists. 2020. High-resolution microstructural and compositional analyses of shock deformed apatite from the peak ring of the Chicxulub impact crater. *Meteoritics & Planetary Science* 19 p. https://doi.org/10.1111/maps.13541.

Deutsch A., Poelchau M., and Kenkmann T. 2015. Impact metamorphism in terrestrial and experimental cratering events. In *EMU notes in mineralogy—Volume 15 Planetary mineralogy*, edited by Lee M. R. and Leroux H. London: European Mineralogical Union and the Mineralogical Society of Great Britain & Ireland. pp. 89–127.

Emmons R. C. 1943. The universal stage (with five axes of rotation). *Geological Society of America Memoir* 8:205p.

Engelhardt W. von and Bertsch W. 1969. Shock induced planar deformation structures in quartz from the Ries crater, Germany. *Contributions to Mineralogy and Petrology* 20:203–234.

Fel'dman V. I. 1994. The conditions of shock metamorphism. In *Large meteorite impacts and planetary evolution*, edited by Dressler B. O. Grieve R. A. F. and Sharpton V. L. Geological Society of America Special Paper 293. Boulder, Colorado: Geological Society of America. pp. 121–132.

Ferrière L., Koeberl C., Ivanov B. A., and Reimold W. U. 2008. Shock metamorphism of Bosumtwi impact crater rocks, shock attenuation, and uplift formation. *Science* 322:1678–1681.

Ferrière L., Morrow J. R., Amgaa T., and Koeberl C. 2009a. Systematic study of universal-stage measurements of planar deformation features in shocked quartz: Implications for statistical significance and representation of results. *Meteoritics & Planetary Science* 44:925–940.

Ferrière L., Koeberl C., and Reimold U. W. 2009b. Characterisation of ballen quartz and cristobalite in impact breccias: New observations and constraints on ballen formation. *European Journal of Mineralogy* 21:203–217.

Ferrière L. and Osinski G. R. 2013. Shock metamorphism. In *Impact cratering: Processes and products*, edited by Osinski G. R. and Pierazzo E. Chichester, UK: Blackwell Publishing Ltd. pp. 106–124.

Folco L., Mugnaioli E., Gemelli M., Masotta M., and Campanale F. 2018. Direct quartz-coesite transformation in shocked porous sandstone from Kamil crater (Egypt). *Geology* 46:739–742.

French B. M. 1998. Traces of catastrophe: A handbook of shock-metamorphic effects in terrestrial meteorite impact structures. LPI Contribution 954. Houston, Texas: Lunar and Planetary Institute. 120 p.

French B. M. and Koeberl C. 2010. The convincing identification of terrestrial meteorite impact structures: What works, what doesn't, and why. *Earth-Science Reviews* 98:123–170.

French B. M. and Short N. M. 1968. *Shock metamorphism of natural materials*. Baltimore, Maryland: Mono Book Corporation. 644 p.

Goltrant O., Cordier P., and Doukhan J.-C. 1991. Planar deformation features in shocked quartz: A transmission electron microscopy investigation. *Earth and Planetary Science Letters* 106:103–115.

Goltrant O., Leroux H., Doukhan J.-C., and Cordier P. 1992. Formation mechanisms of planar deformation features in naturally shocked quartz. *Physics of the Earth and Planetary Interiors* 74:219–240.

Grieve R. A. F. and Alexopoulos J. 1988. Microscopic planar features in quartz from Scollard Canyon, Alberta, and the Cretaceous-Tertiary boundary event. *Canadian Journal of Earth Science* 25:1530–1534.

Grieve R. A. F., Langenhorst F., and Stöffler D. 1996. Shock metamorphism of quartz in nature and experiment: II. Significance in geoscience. *Meteoritics & Planetary Science* 31:6–35.

Gulick S., Christeson G., Barton P., Grieve R., Morgan J., and Urrutia-Fucugauchi J. 2013. Geophysical characterization of the Chicxulub impact crater. *Reviews of Geophysics* 51:31–52.

Hand E. 2016. Updated: Drilling of dinosaur-killing impact crater explains buried circular hills. *Science Magazine*. https://doi.org/10.1126/science.aaf5684

Hildebrand A. R., Penfield G. T., Kring D. A., Pilkington M., Camargo Z. A., Jacobsen S. B., and Boynton W. V. 1991. Chicxulub crater: A possible Cretaceous/Tertiary boundary impact crater on the Yucatán Peninsula, Mexico. *Geology* 19:867–871.

Holm-Alwmark S., Ferrière L., Alwmark C., and Poelchau M. H. 2018. Estimating average shock pressures recorded by impactite samples based on universal stage investigations of planar deformation features in quartz—Sources of error and recommendations. *Meteoritics & Planetary Science* 53:110–130.

Hörz F. 1968. Statistical measurements of deformation structures and refractive indices in experimentally shock loaded quartz. In *Shock metamorphism of natural materials*, edited by French B. M. and Short N. M. Baltimore, Maryland: Mono Book Corporation. pp. 243–253.

Izett G. A. 1990. *The Cretaceous/Tertiary boundary interval, Raton Basin, Colorado and New Mexico*. Geological Society of America Special Paper 249. Boulder, Colorado: Geological Society of America. 100 p.

Kieffer S. W., Phakey P. P., and Christie J. M. 1976. Shock processes in porous quartzite: Transmission electron microscope observations and theory. *Contributions to Mineralogy and Petrology* 59:41–93.

Kowitz A., Schmitt R. T., Reimold W. U., and Hornemann U. 2013a. The first MEMIN shock recovery experiments at low shock pressure (5–12.5 GPa) with dry, porous sandstone. *Meteoritics & Planetary Science* 48:99–114.

Kowitz A., Güldemeister N., Reimold W. U., Schmitt R. T., and Wünnemann K. 2013b. Diaplectic quartz glass and SiO_2 melt experimentally generated at only 5 GPa shock pressure in porous sandstone: Laboratory observations and meso-scale numerical modeling. *Earth and Planetary Science Letters* 384:17–26.

Kowitz A., Güldemeister N., Schmitt R. T., Reimold W. U., Wünnemann K., and Holzwarth A. 2016. Revision and recalibration of existing shock classifications for quartzose rocks using low-shock pressure (2.5–20 GPa) recovery experiments and mesoscale numerical modeling. *Meteoritics & Planetary Science* 51:1741–1761.

Kring D. A., Tikoo S. M., Schmieder M., Riller U., Rebolledo-Vieyra M., Simpson S. L., Osinski G. R., Gattacceca J., Wittmann A., Verhagen C. M., Cockell C. S., Coolen M. J. L., Longstaffe F. J., Gulick S. P. S., Morgan J. V., Bralower T. J., Chenot E., Christeson G. L., Claeys P., Ferrière L., Gebhardt C., Goto K., Green S. L., Jones H., Lofi J., Lowery C. M., Ocampo-Torres R., Perez-Cruz L., Pickersgill A. E., Poelchau M. H., Rae A. S. P., Rasmussen C., Sato H., Smit J., Tomioka N., Urrutia-Fucugauchi J., Whalen M. T., Xiao L., and Yamaguchi K. E. 2020. Probing the hydrothermal system of the Chicxulub impact crater. *Science Advances*. 6: eaaz3053. https://doi.org/10.1126/sciadv.aaz3053.

Losiak A., Golebiowska I., Ferrière L., Wojciechowski J., Huber M. S., and Koeberl C. 2016. WIP: A web-based program for indexing planar features in quartz grains and its usage. *Meteoritics & Planetary Science* 51:647–662.

Mansfeld U., Langenhorst F., Ebert M., Kowitz A., and Schmitt R. T. 2017. Microscopic evidence of stishovite generated in low-pressure shock experiments on porous sandstone: Constraints on its genesis. *Meteoritics & Planetary Science* 52:1449–1464.

Morgan J., Lana C., Kearsley A., Coles B., Belcher C., Montanari S., Diaz-Martinez E., Barbosa A., and Neumann V. 2006. Analyses of shocked quartz at the global K-P boundary indicate an origin from a single, high-angle, oblique impact at Chicxulub. *Earth and Planetary Science Letters* 251:264–279.

Morgan J. V., Gulick S. P. S., Bralower T., Chenot E., Christeson G., Claeys P., Cockell C., Collins G. S., Coolen M. J. L., Ferrière L., Gebhardt C., Goto K., Jones H., Kring D. A., Le Ber E., Lofi J., Long X., Lowery C., Mellett C., Ocampo-Torres R., Osinski G. R., Perez-Cruz L., Pickersgill A., Pölchau M., Rae A., Rasmussen C., Rebolledo-Vieyra M., Riller U., Sato H., Schmitt D. R., Smit J., Tikoo S., Tomioka N., Urrutia-Fucugauchi J., Whalen M., Wittmann A., Yamaguchi K. E., and Zylberman W. 2016. The formation of peak rings in large impact craters. *Science* 354:878–882.

Morgan J., Gulick S., Mellet C. L., and Green S. L. and the Expedition 364 Scientists. 2017. *Chicxulub: Drilling the K-Pg impact crater*. Proceedings of the International Ocean Discovery Program, 364. College Station, Texas: International Ocean Discovery Program. 164 p.

Müller W. F. and Défourneaux M. 1968. Deformationsstrukturen-im Quarz als Indikator für Stosswellen: Eine experimentelle Untersuchung an Quartz-Einkristallen. *Zeitschrift für Geophysik* 34:483–504.

Nakano Y., Goto K., Matsui T., Tada R., and Tajika E. 2008. PDF orientations in shocked quartz grains around the Chicxulub crater. *Meteoritics & Planetary Science* 43:745–760.

Penfield G. T. and Camargo Z. A. 1981. Definition of a major igneous zone in the central Yucatán platform with aeromagnetics and gravity. *Society of Exploration Geophysicists Technical Program, Abstracts, and Biographies* 51:37.

Pittarello L., Ferrière L., Feignon J.-G., Osinski G. R., and Koeberl C. 2020. Preferred orientation distribution of shock-induced planar microstructures in quartz and feldspar. *Meteoritics & Planetary Science* 55:1082–1092.

Poelchau M. H. and Kenkmann T. 2011. Feather features: A low-shock-pressure indicator in quartz. *Journal of Geophysical Research* 116:B02201.

Rae A. S. P., Collins G. S., Poelchau M., Riller U., Davison T. M., Grieve R. A. F., Osinski G. R., Morgan J. V., and IODP-ICDP Expedition 364 Scientists. 2019. Stress-strain evolution during peak-ring formation: A case study of the Chicxulub impact structure. *Journal of Geophysical Research: Planets* 124:396–417.

Riller U., Poelchau M. H., Rae A. S. P., Schulte F. M., Collins G. S., Melosh H. J., Grieve R. A. F., Morgan J. V., Gulick S. P. S., Lofi J., Diaw A., McCall N., Kring D. A., and IODP-ICDP Expedition 364 Science Party. 2018. Rock fluidization during peak-ring formation of large impact structures. *Nature* 562:511–518.

Schmieder M., Kring D. A., and the IODP-ICDP Expedition 364 Science Party. 2017. Petrology of target dolerite in the Chicxulub peak ring and a possible source of K/Pg boundary picotite spinel (abstract #1964). 48th Lunar and Planetary Science Conference. CD-ROM.

Schmieder M., Erickson T. M., and Kring D. A. and the IODP-ICDP Expedition 364 Science Party. 2019. Microstructural characterization of TiO_2-II in the chicxulub peak ring (abstract #1568). 50th Lunar and Planetary Science Conference. CD–ROM.

Schulte P., Alegret L., Arenillas I., Arz J. A., Barton P. J., Bown P. R., Bralower T. J., Christeson G. L., Claeys P., Cockell C. S., Collins G. S., Deutsch A., Goldin T. J., Goto K., Grajales-Nishimura J. M., Grieve R. A. F., Gulick S. P. S., Johnson K. R., Kiessling W., Koeberl C., Kring D. A., MacLeod K. G., Matsui T., Melosh J., Montanari A., Morgan J. V., Neal C. R., Nichols D. J., Norris R. D., Pierazzo E., Ravizza G., Rebolledo-Vieyra M., Reimold W. U., Robin E., Salge T., Speijer R. P., Sweet A. R., Urrutia-Fucugauchi J., Vajda V., Whalen M. T., and Willumsen P. S. 2010. The Chicxulub asteroid impact and mass extinction at the Cretaceous-Paleogene boundary. *Science* 327:1214–1218.

Sharpton V. L., Dalrymple G. B., Marin L. E., Ryder G., Schuraytz B. C., and Urrutia-Fucugauchi J. 1992. New links between the Chicxulub impact structure and the Cretaceous/Tertiary boundary. *Nature* 359:819–821.

Smit J. 1999. The global stratigraphy of the Cretaceous-Tertiary boundary impact ejecta. *Annual Review of Earth and Planetary Sciences* 27:75–113.

Sprain C. J., Renne P. R., Clemens W. A., and Wilson G. P. 2018. Calibration of chron C29r: New high-precision geochronologic and paleomagnetic constraints from the Hell Creek region, Montana. *Geological Society of America Bulletin* 130:1615–1644.

Stöffler D. 1972. Deformation and transformation of rock-forming minerals by natural and experimental shock processes. I. Behavior of minerals under shock compression. *Fortschritte der Mineralogie* 49:50–113.

Stöffler D. and Langenhorst F. 1994. Shock metamorphism of quartz in nature and experiment: I. Basic observation and theory. *Meteoritics* 29:155–181.

Stöffler D., Hamann C., and Metzler K. 2017. Shock metamorphism of planetary silicate rocks and sediments: Proposal for an updated classification system. *Meteoritics & Planetary Science* 53:5–49.

Timms N. E., Pearce M. A., Erickson T. M., Cavosie A. J., Rae A. S. P., Wheeler J., Wittman A., Ferrière L., Poelchau M. H., Tomioka N., Collins G. S., Gulick S. P. S., Rasmussen C., Morgan J. V., IODP-ICDP Expedition 364 Scientists. 2019. New shock microstructures in titanite ($CaTiSiO_5$) from the peak ring of the Chicxulub impact structure, Mexico. *Contributions to Mineralogy and Petrology* 174:38. https://doi.org/10.1007/s00410-019-1565-7.

Trepmann C. A. and Spray J. G. 2005. Planar microstructures and Dauphiné twins in shocked quartz from the Charlevoix impact structure, Canada. In *Large meteorite impacts III*, edited by Kenkmann T., Hörz F., and Deutsch A. Geological Society of America Special Paper 384. Boulder, Colorado: Geological Society of America. pp. 315–328.

Trepmann C. A. and Spray J. G. 2006. Shock-induced crystal-plastic deformation and post-shock annealing of quartz: Microstructural evidence from crystalline target rocks of the Charlevoix impact structure, Canada. *European Journal of Mineralogy* 18:161–173.